Influence of dynamic crosslinking on the morphology, crystallization, and dynamic mechanical properties of PA6,12/EVA blends

Fabrício Bondan,[1] Juliano Roberto Ernzen,[2] Javier Amalvy,[3,4] Ana Vera Machado,[5] Johnny De Nardi Martins,[6] Otávio Bianchi[1]

[1]Programa de Pós-Graduação Em Engenharia e Ciência dos Materiais-PGMAT, Universidade de Caxias do Sul, Rua Francisco Getúlio, Vargas 1130, Bloco V, Caxias Do Sul, Brazil

[2]Mantova Indústria de Tubos Plásticos Ltda, Caxias Do Sul, Brazil

[3]Instituto de Investigaciones Fisicoquímicas Teóricas y Aplicadas (INIFTA), Argentina

[4]FRLP-UTN, Centro de Investigación y Desarrollo en Ciencia y Tecnologia de Materiales (CITEMA), La Plata, Argentina

[5]Institute for Polymers and Composites, University of Minho, Portugal

[6]Campus Blumenau, Universidade Federal de Santa Catarina, Blumenau, Brazil

Correspondence to: O. Bianchi (E-mail: otavio.bianchi@gmail.com)

ABSTRACT: This study investigated the effect of dynamic crosslinking of polyamide 6,12 and random copolymers of ethylene and vinyl acetate blends (PA6,12/EVA) on the morphology, crystallinity, and dynamic mechanical properties. The crosslinking agent was dicumyl peroxide (DCP), and the blends were processed in a torque rheometer. The morphology depended on the DCP content, and all blends exhibited the same crystallinity index. However, with increasing crosslinking degree, the interfacial tackiness (E) values increased from 1.8 to 2.7 nm. The lamellar structures of all blends started forming at approximately 160 °C, close to the temperature of pure polyamide. The crosslinked phase enhanced the pseudo-elastic behavior of the blends and increased their molecular mobility activation energy. Samples with higher crosslinking degree exhibited smaller permanent deformation (0.01%) than those with low crosslinking. © 2016 Wiley Periodicals, Inc. J. Appl. Polym. Sci. **2016**, *133*, 44206.

KEYWORDS: elastomers; polyamides; structure-property relations; synthesis and processing; thermoplastics

DOI: 10.1002/app.44206

INTRODUCTION

Thermoplastic vulcanizates (TPVs) are a class of thermoplastic elastomers which combines the processability of thermoplastics with the properties of crosslinked/vulcanized rubber.[1,2] The mechanical, thermal properties, and chemical behavior of these materials are a result of the phase morphology developed during processing.[3,4] TPVs are produced by dynamic vulcanization/crosslinking, wherein the elastomeric and thermoplastic phases crosslink during melt processing.[5–9] These materials can be prepared using conventional thermoplastic processing equipment and are also reprocessed and recyclable.[1] The combined characteristics of TVEs have been exploited in a variety of applications such as automobiles, civil construction, and wiring and cable coating.[10] Once the three-dimensional network of the elastomeric phase is formed by chemical reactions, the morphology of the polymer blends stabilizes, and the TPV final morphology is formed. The shear stresses originating in the batch mixers or twin screw extruder during melt processing nearly always fragment the elastomeric phase into small particles (1–5 μm). These fragments are partially insoluble in organic solvents.[4,6,7,11–13] The final properties of these materials largely depends on the diffusion of processing aids,[14] phase inversion[15] and compatibilization,[16] crystallization conditions of semicrystalline components,[17,18] morphology stabilization,[19] processing conditions,[19] rheological and viscoelastic conditions of the mixing process.[13,20,21]

The crosslinking of ethylene vinyl acetate (EVA) with various thermoplastics occurs in the presence of organic peroxides. In the literature, EVA has been blended with linear low-density polyethylene,[22] low-density polyethylene,[23] high-density polyethylene,[24] polypropylene,[25] and polyamide 12 (PA12).[6] EVA crosslinking has also been achieved by thermal decomposition in dicumyl peroxide (DCP).[15,16] The radicals generated by homolytic scission of DCP mainly abstract the hydrogen attached to the tertiary carbons of EVA, forming macroradicals in the

polymer chain. The macroradicals combine to form new C–C bonds among the polymer chains, generating the crosslinked phase.[6,7]

In many polymer blends, the promotion of crosslinking by specific agents provides an alternative means of stabilizing the phase morphology.[5–7,9,26,27] Other stabilization techniques involve nanoparticles and specific polymer–polymer interactions.[28–33] Na *et al.*[34] noted that the presence of EVA in the HDPE/EVA blends increases the size of the lamellar structure without changing the melting temperatures of the individual components. Balamurugan and Maiti[35] showed that the crystallization kinetics of nonisothermal crystallized polyamide-6 (PA6) blended with a copolymer of butyl ethylene-co-acrylate (EBA) are influenced by the applied high cooling rates. Thus, the inclusion of elastomeric particles EBA may slightly hamper the motions of the PA6 molecular chains or slightly alter the extent of the grown PA6 crystals. In PA6/EVA blends compatibilized with maleic anhydride (MA),[14] the content of EVA increases up to 30 wt % of pure PA6. The addition of EVA reduces the crystalline lamella values and consequently increases the amorphous lamella. Bondan and Soares[6] studied PA12/EVA blends dynamically crosslinked with DCP and showed that the DCP exerts almost no effect on the polyamide properties. In contrast, they later showed that the morphologies and tensile strain behaviors in 50/50 PA6,12/EVA blends depend on the DCP content.[5]

This article aims to investigate the relationship between the dynamic crosslinking of PA6,12/EVA blends and their morphology, crystallinity, and dynamic mechanical properties. We focused on the effect of dynamical crosslinking on the polymer–polymer interfacial thickness, crystallization behavior of PA6,12 in the blends, and the solid viscoelastic properties. Additionally, we examined the interfacial thickness of the blends as a function of the crosslinking agent content and related this thickness to the solid viscoelastic behavior.

EXPERIMENTAL

Materials

The ethylene vinyl acetate (EVA) copolymer was supplied by Braskem Co. (8019 PE). By thermogravimetric analysis (TGA), the vinyl acetate content, MFI, and density of EVA were determined as 27.5 wt %, 6 g/10 min (190 °C/2.16 kg), and 0.95 g cm^{-3}, respectively. Polyamide 6,12 (PA6,12; density = 1.11 g cm^{-3}) was supplied by UBE Engineering Plastics S.A (7034B), code 331Z26. All polymers have been previously subjected to thermogravimetry experiments to evaluate its thermal degradation profile (shown in Supporting Information). Dicumyl peroxide (DCP) (98% purity) was used as received by Retilox Química Especial. Prior to melt processing, all polymers were dried in a vacuum oven at 50 °C for 24 h.

Methods

Processing. PA6,12/EVA blends with different EVA weight fractions (0.1–0.5) were processed in a torque rheometer (Haake Rheomix 600p) using a 75 cm^3 mixing chamber with counter-rotating roller rotors. The materials were prepared at 200 °C for 15 min at 120 rpm. The dynamic crosslinked blends were prepared from different amounts of DCP (0, 1, 4, and 8 parts per hundred of rubber/elastomer (phr), relative to the EVA contents). First, PA6,12 and EVA pellets were placed in the hot mixer chamber. These materials were mixed into a homogeneous melt. The fluid was considered homogenous when $\frac{d\text{torque}}{dt} \sim 0$ (around 5 min). Next, DCP was added, and mixing was kept up to 15 min. Blends without DCP were processed by the same procedure. Rectangular bars of dimensions 40 mm × 10 mm × 3.2 mm were prepared by injection molding in a Haake mini-injection II and retained for characterization analyses.

Gel Content and Selective Extraction. The crosslinking degrees of pure EVA and PA6,12/EVA blends were estimated through the gel contents (insoluble EVA fraction), following the procedure based on the ASTM 2765 standard. A 120-mesh wire cage containing approximately 0.3 g of ground polymer (30–60 mesh) was washed in a round-bottomed flask containing boiling *m*-cresol for 8 h, as previously described.[7,20] After solvent extraction, all samples were dried at 60 °C for 48 h. The gel content was estimated as follows:

$$\text{GelContent}(\%) = \frac{W_f}{W_i} 100, \quad (1)$$

where W_i and W_f are the initial and final (dried) polymer weights, respectively.

The co-continuity region was determined by a solvent-selective extraction technique. The solubility parameters of EVA (9.27 $(cal/cm^3)^{1/2}$) and PA6,12 [9.54 $(cal/cm^3)^{1/2}$] used in this work were approximated from Fedors' molar volume.[36] The EVA phase was dissolved in xylene, selected for its similar solubility (8.80 cal/cm^3) to EVA.[37] The samples were placed in the 120-mesh wire cage containing approximately 0.3 g of polymer and washed in a round-bottomed flask containing boiling xylene for 8 h. After solvent extraction, all samples were dried at 60 °C for 48 h. The continuity of one phase is defined as the fraction of the continuous phase. The continuity of polymer A (PA6,12) is evaluated as follows:

$$\text{Continuity}(\%) = \frac{W_i - W_f}{\phi_{\text{PA6,12}} W_i} .100 \quad (2)$$

where W_i and W_f denote the initial (pre-extraction) and final (postextraction) weights of the polymer, respectively, and $\phi_{\text{PA6,12}}$ is the weight fraction of PA6,12.

Morphology. The morphologies of the blends were investigated by scanning electron microscopy (SEM) using a Shimadzu SSX-550. Small samples (30 mm × 3 mm × 1 mm) from the central core of the injection-molded bars were cryofractured and immersed in hot xylene for 1 h to remove the EVA phase and reveal the phase boundaries of the uncrosslinked blends. All samples were sputter coated with gold before imaging.

The number average diameter ($\overline{D_n}$), weight average diameter ($\overline{D_w}$), volume average diameter ($\overline{D_v}$), and polydispersity index (PID) $\left(\overline{D_w}/\overline{D_n}\right)$ of the EVA phase of the blends with dispersed-phase morphology were, respectively, estimated as follows[38]:

$$\overline{D}_n = \frac{\sum N_i D_i}{\sum N_i}, \quad (3)$$

$$\overline{D}_w = \frac{\sum N_i D_i^2}{\sum N_i D_i}, \quad (4)$$

$$\overline{D}_v = \frac{\sum N_i D_i^4}{\sum N_i D_i^3}, \quad (5)$$

where N_i is the number of domains with diameter D_i.

The droplet size was determined by digital image analysis using the freeware software Image Tool, version 3.00 (UTHSCSA). At least three micrographs were analyzed in each case.[39]

Attenuated Total Reflectance–Fourier Transform Infra-Red Spectroscopy (ATR-FTIR). The chemical interactions in the PA6,12/EVA blends were evaluated by Fourier transform infrared spectroscopy (FTIR) analysis using a Perkin Elmer Impact 400 spectrometer in attenuated total reflectance (ATR) mode. The measurements were performed at 1 cm^{-1} resolution with 32 scans from 4000 to 400 cm^{-1}.

Synchrotron Small-Angle X-ray Scattering (SAXS). SAXS experiments were performed on the SAXS1 beamline of the Brazilian Synchrotron Light Laboratory (LNLS), monitored with a photomultiplier, and detected on a Pilatus (300 k, 84 mm × 107 mm) positioned at 836 mm. The generated scattering wave vectors (q) ranged from 0.13 to 2.5 nm^{-1}. The wavelength of the incident X-ray beam (λ) was 0.155 nm. Background and parasitic scatterings were determined by separate measurements in an empty holder and subtracted from the raw SAXS results.

Interfacial Thickness of PA6,12/EVA Blends. According to Porod's law, the scattering intensity [$I(q)$] of the SAXS curve of a sample with coarse phase contours decreases as q^{-4}. Polymeric materials deviate from Porod's law because their product $I(q).q^4$ is not constant. Ruland[40] analyzed the deviations from Porod's law in a model of two phases connected by a transition layer. By analyzing the deviation of the scattering curve at large q, we can determine the specific interfacial area (S/V) and size of the interface. In an ideal system, that is, a two-phase model with no measurable thickness, $I(q_{id})$ follows Porod's law at large q and decreases as a function of q^4. In the large q limit, the scattering intensity should be proportional to the total area (S) of the boundaries between the two phases in the scattering volume. This relationship is expressed as eq. (5), where $\Delta\rho$ is the electron density difference between the two phases[41,42]:

$$\lim_{q\to\infty}[I_{id}(q)] = \frac{2\pi(\Delta\rho)^2 S}{q^4}. \quad (6)$$

In the present study, the thickness of the PA6,12–EVA interface was measured at 200 °C (processing temperature) using a Linkam DSC600. Initially, the disk-shaped samples (of diameter and thickness 7 mm and 1 mm, respectively) were heated to 220 °C at 10 °C min^{-1} and maintained at that temperature for 10 min to erase their thermal history. Subsequently, the samples were cooled to 200 °C for measurements. The interfacial thickness was determined from the electronic contrast scattering of a two-phase system, as described in the literature.[42,43]

Effect of EVA on PA6,12 Crystallization. The lamellar long period (L_p) can be estimated from the Bragg relationship [eq. (7)]. The lamellar long period is associated with the formation of long-range planning structures of polymers and is inversely proportional to the maximum vector magnitude of the peak scattering (q_{max})[44]:

$$L_P = \frac{2\pi}{q_{Max}} \quad (7)$$

Differential Scanning Calorimeter (DSC). DSC analyses were performed in a DSC 50 Shimadzu under a nitrogen atmosphere with a flow rate of 50 mL min^{-1}. The samples (10 mg) were heated at 10 °C min^{-1} to 220 °C and kept at this temperature for 3 min to erase their thermal history. The samples were then cooled to room temperature at 10 °C min^{-1}. The degree of crystallinity (X_c) was calculated as follows[45]:

$$X_c = \frac{\Delta H_f}{\Delta H_f^{\circ}.\phi_{PA6,12}}.100, \quad (8)$$

where ΔH_f is the melting enthalpy of fusion of the samples (J/g), ΔH_f° is the theoretical melting enthalpy of 100% crystalline PA6,12 (197J/g),[46] and $\phi_{PA6,12}$ is the mass fraction of PA6,12 in the blends.

Dynamic Mechanical Thermal Analysis (DMTA). Dynamic mechanical experiments of the PA6,12/EVA blends were performed in a DMA 242C (Netzsch) using single cantilever geometry. The experiments were the linear viscoelastic region at small amplitude (30 μm) in the temperature range of 150 to 100 °C. The heating rate was fixed at 3 °C min^{-1}, and the frequency was set to 1, 5, 10, 20, and 50 Hz for all samples. The samples were rectangular bars sized 16 mm × 10 mm × 3.2 mm and cut from the injection-molded bar specimens.

The creep and recovery behaviors were investigated in the DMA 242C (Netzsch) using compression geometry. Cubic samples (2 mm × 2 mm × 2 mm) were maintained at 70 °C (PA6,12 and blends) or 50 °C (pure EVA) for 30 min to equilibrate the temperature. In the creep measurements, the displacement was set to 7 N for 30 min. The recovery time was set to 30 and 42 min at 70 and 50 °C, respectively.

RESULTS AND DISCUSSION

Melt Processing and Crosslink Degree

The addition of dicumyl peroxide to PA6,12/EVA blends increased the stabilized torques. Bondan and Soares confirmed this trend in the dynamic crosslinking of the PA12/EVA and PA6,12/EVA blends prepared in a mixing chamber.[5,6]

The stabilized torque was also improved by increasing the DCP proportion in EVA (see Table I). This trend was attributed to the higher amount of free radical in the reaction medium, which increases the viscosity. However, the stabilized torque of PA6,12 was insensitive to DCP addition, regardless of content. This indicates the DCP is more selectively to EVA.[5] Similar results, in which DCP more easily forms crosslinks in the EVA phase than in the PA phase have been reported in the literature.[6] This trend was due to the greater amount of tertiary carbons in the EVA structure when compared to the polyamide chains.[5,6,15]

Table I. Stabilized Torque and Melt Viscosity Data of EVA and PA6,12 with Increasing Amount of DCP Crosslinker

Sample	DCP (phr)	T (N m)	η (Pa s)
EVA	0	4.1	323
	1	10.4	818
	4	20.1	1577
	8	32.1	2528
PA6,12	0	11.6	916
	1	12.4	974
	4	12.8	1006
	8	13.9	1096

At temperatures above 120 °C, the O–O bond of DCP undergoes homolysis, forming primary cumiloxy radicals and secondary methyl radicals.[19] Because of the numerous tertiary carbons in the EVA copolymer, hydrogen abstraction via free radicals is a very probable reaction.[8,15,16] After the formation of free radicals, hydrogen atoms are abstracted from the polymer chain. This radical is transferred from peroxide, generating a macroradical in the polymer backbone. In the third step, the polymeric macroradicals recombine to form new covalent bonds (C–C) between the chains, increasing their molecular weight and viscosity.

The melt viscosity η was estimated by Bousmina *et al.*'s model based on a Couette analogy[47]:

$$\eta = \frac{T}{N}\frac{(\beta^2-1)}{8\pi^2 L R_e^2 (1+g^2)}. \quad (9)$$

Here, T is the stabilized torque, and $\beta = R_e/R_i$, where R_e is the radius of the chamber and R_i is the equivalent internal radius of the rotor blades. Also, N is the applied rotor speed, and $g = N_2/N_1$ is the ratio of the second (N_2) to first (N_1) rotor blade speeds (note that N_1 is the applied rotor speed N, i.e., $N_1 = N$).Here, L is the length of the rotors.[47] For the mixer chamber, we selected $R_e = 20$ mm, $L = 48$ mm, $R_i = 17.6$ mm, and $g = 2/3$. In this approach, the two rotor blades in a batch mixer are assumed equivalent to two adjacent Couette cells with the same external radius and effective internal hydrodynamic radius, rotating at the same angular speed and exerting the same torque.[47]

The melt viscosities of the EVA samples increased proportionally to the amount of DCP added (see Table I). These results reflect the formation of new covalent bonds (C–C) between the chains as previously discussed. The melt viscosity changes were small in PA6,12 because DCP does not readily react with this polymer.

The gel content in the EVA increased proportionally to the DCP content, as shown in Figure 1. A trend line (B-spline) has been added to help the experimental data elucidation. In contrast, PA6,12 formed no detectable gel structures in the presence of DCP, as also observed for PA12.[6] The formation of the crosslinked structures increased with increasing DCP content. The gel content (indicating the extent of crosslinked networks) comprised 0 wt % in blends without DCP, 2.6 wt % in blends containing 1 phr DCP, and 17 wt % in blends containing 4 phr DCP. In blends containing 8 phr, the DCP content was excessive; so, the gel content decreased to 10.5 wt %. If the number of DCP-generated radicals in the polymer interface becomes very high, the three-dimensional network in the EVA phase is inhibited.[19] Bianchi *et al.*[48] showed that over 90 wt % gel in EVA can be achieved by just 2 phr of DCP. On the other hand, some of the DCP is lost by direct blending with polyamide in the dynamic processing.

Morphology

Blends of two polymers typically produce an immiscible system with a distinct two-phase morphology. The morphologies of the immiscible systems depend on their compositions. Generally, polymer blends with concentrations near equivalence present a co-continuous phase morphology.[13]

Immiscibility is a typical property of elastomer–polyamide blends and is exemplified by PA12/EVA[6] and PA6/EVA[14] blends, which are immiscible even under low interfacial tension (0.63 mN/m in the former case). The size of the phases is directly associated with the interfacial tension between the blend components and can be reduced by compatibilizing the polymer blends to reduce their interfacial tension. The developed morphology also depends on the melt viscosity ratio of the constituents.[49] The greater the melt viscosity difference in a dispersed phase system is, the smaller the size of the dispersed phase is.[25,50]

The number average domain size ($\overline{D_n}$) increased with increasing EVA content in the PA6,12/EVA blends, while the $\overline{D_w}/\overline{D_n}$ remained almost constant. The $\overline{D_n}$ increased from 0.64 μm at 10 wt % EVA to 1.57 μm at 30 wt % EVA (see Table II). The 50/50 blends were completely co-continuous; so, their domain sizes could not be measured (Figure 2).

Figure 2 presents the amount of co-continuous phase as a function of the weight fraction of EVA. Interconnected phases comprised 16 wt % of mixtures containing 30 wt % EVA. In 40 wt % EVA blends and 50/50 blends, the continuous phases increased to 46.5 and 99 wt %, respectively.

Interfacial tensions can be determined from the surface tensions of the pure components. In this work, the interfacial tension

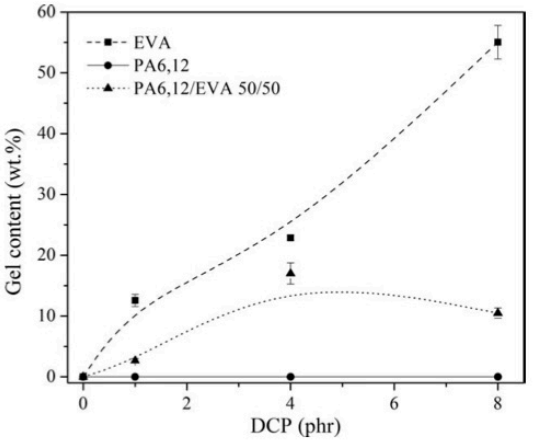

Figure 1. Gel content as a function of DCP amount in pure polymers and blends.

Table II. Number Average Diameter ($\overline{D_n}$), Weight Average Diameter ($\overline{D_w}$), Volume Average Diameter ($\overline{D_v}$), and Polydispersity index (PDI) ($\overline{D_w}/\overline{D_n}$) of the EVA Phase Dispersed in the PA6-12 Matrix

PA6-12/EVA	$\overline{D_n}$ (μm)	$\overline{D_w}$ (μm)	$\overline{D_v}$ (μm)	$\overline{D_w}/\overline{D_n}$
90/10	0.64	0.69	0.80	1.08
80/20	1.31	1.46	1.78	1.11
70/30	1.57	1.75	2.08	1.11

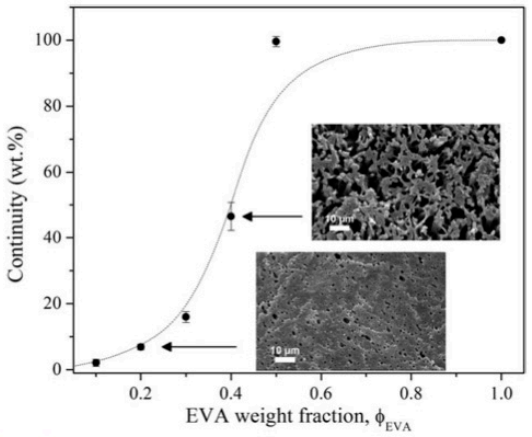

Figure 2. Effect of composition on the co-continuous blend morphology of PA6,12/EVA blends.

was estimated as the geometric mean of the well-known Owens and Wendt equation,[51] which describes the tension between low-energy and high-energy materials:

$$\gamma_{12}=\gamma_1+\gamma_2-2\sqrt{\gamma_1^d\gamma_2^d}-2\sqrt{\gamma_1^p\gamma_2^p} \quad (10)$$

In eq. (10), the superscripts d and p refer to the dispersive and polar contributions, respectively, of PA6,12 (subscript 1) and EVA (subscript 2). Given that the blends were prepared at 200 °C and that the surface tension is temperature dependent, the interfacial surface tension γ_{12} at the melt temperature was determined by Guggenheim's equation[52]:

$$\gamma=\gamma(0)\left(1-\frac{T}{T_c}\right)^{\frac{11}{9}}. \quad (11)$$

The surface tensions at $T=0$ K [$\gamma(0)$] and the imaginary critical temperature (T_c) were taken from the literature.[7,36] According to eq. (11), the surface tension decreases with temperature. The

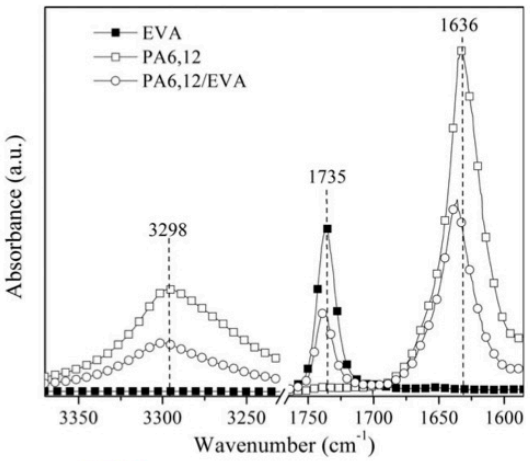

Figure 3. Infrared spectra of PA6-12/EVA blends.

interfacial tension is contributed by both polar and dispersive components, which are usually found at 20 °C. Assuming that both components follow the same temperature dependence as the total surface tension, the polar and dispersive contributions to the polymers at the mixing temperature can be computed by Guggenheim's equation. The EVA copolymer surface energies are listed along with other relevant constants in Table III. These values were estimated by the additive rule based on the weight proportions of ethylene and vinyl acetate in the copolymer. The total, dispersive, and polar components of the surface energy in the EVA sample were similar to those reported in the literature.[6]

The interfacial tension, estimated from the geometric mean of PA6,12 and EVA containing 27.5 wt % vinyl acetate, was 4.62 mN/m, indicating that the PA6,12/EVA blends are thermodynamically incompatible. The weak adhesion between the phases results in large empty spaces on the fractured surface of the particles, as reported in the literature.[38,53]

Figure 3 presents the FTIR spectra of the PA6,12/EVA blends. The peak at 3298 cm^{-1} is attributed to hydrogen bonding among the N–H groups of the polyamide.[31,54,55] When the polymers are blended, the peaks caused by carbonyl (C = O) stretching in EVA appear at different positions (3298, 1735, and 1636 cm^{-1}), reflecting the interactions between the acetate and amide groups in PA6,12 and EVA.

Specific interactions between the N−H and C═O groups in copolyamide/EVA blends were demonstrated by Tsebrenko and Pakharenko.[56] Földes and Pukánszky reported similar specific interactions

Table III. Surface Tension Data of the Components of the Blends at 20 °C

Sample	Total surface energy, γ (mN m^{-1})	Dispersive surface energy, γ_d (mN m^{-1})	Polar surface energy, γ_p (mN m^{-1})	γ(0) (mN m^{-1})	Temperature coefficient $d\gamma/dT$, (mN/m K)	T_c (K)
PA6-12	32.8	27.3	5.48	58.9	−0.065	1018.2
EVA	35.6	32.3	3.3	56.7	−0.067	928.4

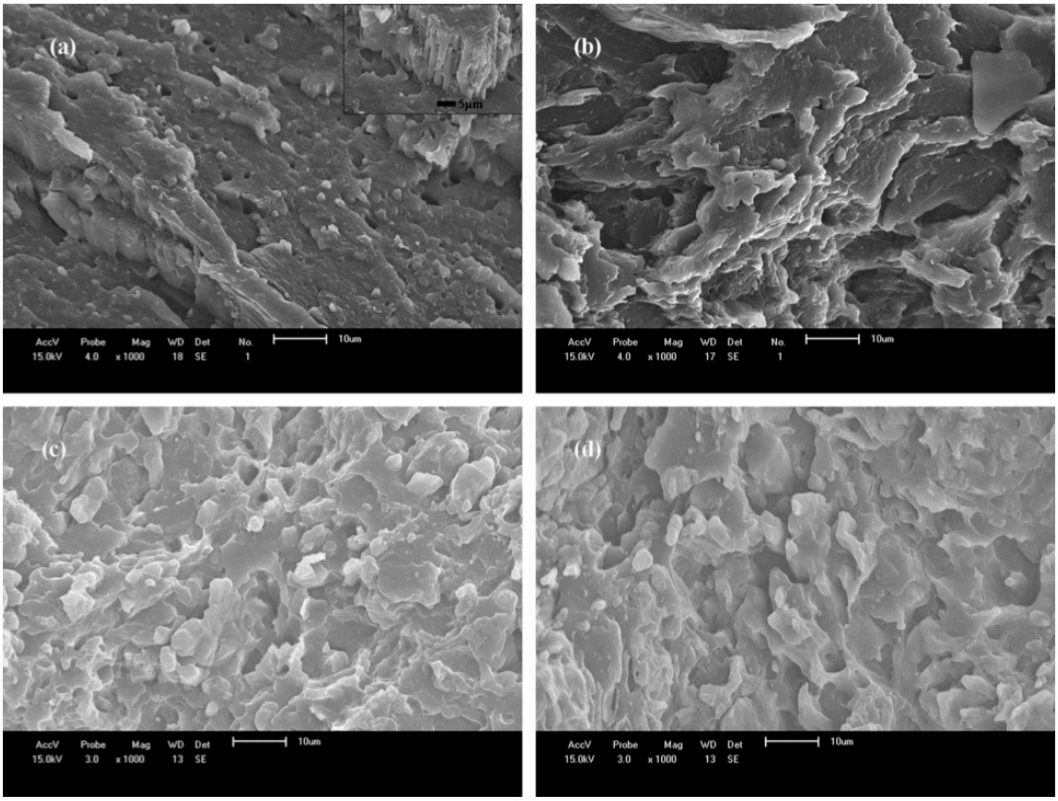

Figure 4. Phase morphologies of polymer blends PA6,12/EVA (a) in the absence of DCP and with addition of (b) 1 phr DCP, (c) 4 phr DCP, and (d) 8 phr DCP.

in ethylene vinyl alcohol copolymer and polyamide 6/66 blends.[54] These specific interactions help to stabilize the phase morphology and finely disperse the polymers,[54] as shown in Figure 2.

Figure 4 shows SEM micrographs of the 50/50 blends with different DCP contents (0, 1, 4, and 8 phr). The morphologies of the PA6,12/EVA blends depended on their DCP contents. The PA6,12/EVA sample without DCP showed a co-continuous phase morphology [Fig. 4(a)]. In the presence of DCP, the crosslinks formed in the EVA phase caused partial fragmentation of the EVA phase [Fig. 4(b)].

The EVA phase was partially fragmented by mechanical forces acting during the melt processing, which increased the melt viscosity by C–C bond formation. The EVA phase fragments at some critical shear stress. Nevertheless, as the DCP-induced crosslinking rate is high at 200 °C,[5] the morphology is stabilized at an early stage,[4] and EVA size cannot be reduced by mechanical forces [Fig. 4(c,d)].

Synchrotron Small-Angle X-ray Scattering (SAXS) and Differential Scanning Calorimeter (DSC)

The scattering intensities $I(q)$ of the PA6,12/EVA blends versus the scattering vector q are plotted in Figure 5. In the amorphous polymers, the scattering intensity curve resembles that of vitreous solids and liquids, with no long-range order.[44,57] Therefore, when measuring the interfacial thickness of the semicrystalline polymer blends, the experimental conditions must ensure no long-range order in the samples.

All samples exhibited similar $I_m(q)$ versus q profiles; namely, the $I_m(q)$ decayed rapidly near one and reduced at higher q. These

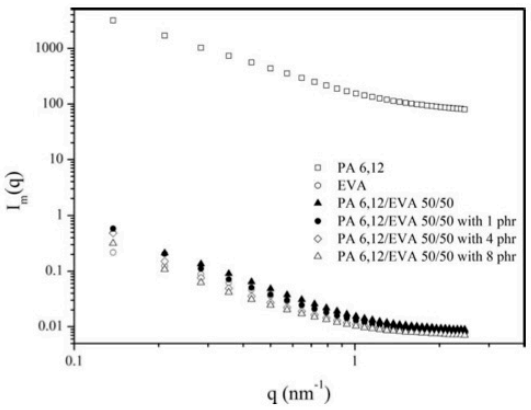

Figure 5. $I_m(q)$ versus q curves for PA6,12, EVA, and blends containing different concentrations of peroxide at 200 °C.

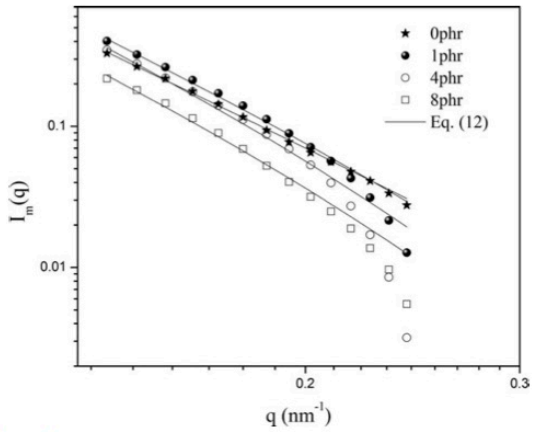

Figure 6. Here, $I_m(q)$ versus q after background subtraction in blends containing different DCP concentrations at 200 °C.

results are attributed to scattering under fluctuations of electron density. Across the range of q, the scattering intensity was higher for PA6,12 than for the other samples because nitrogen electronically contributes to scattering in the liquid sample.

The background scattering, arising from thermal motions of the atoms within the phases, can be matched by the procedure proposed by Vonk.[41,58] This procedure derives an empirical relation among the SAXS curves based on the literature reports.[43]

The interfacial thickness between the polymers at the melt temperature was determined from the corrected scattered intensity $I_{corr}(q)$ obtained by subtracting the background intensity from the measured intensity. The interfacial thickness E was then calculated by Porod's Law.[59,60] The corrected intensity is given by

$$I_{corr}(q) = \frac{K_p}{q^4} e^{(-4\pi^2\sigma^2 q^2)}, \quad (12)$$

where $I_{corr}(q) = I_m(q) - I_{background}$, and K_p is the Porod constant. The parameter σ was determined by a graphical procedure. In this paper, the interfacial thickness ($E = \sqrt{12\sigma}$) was estimated from eq. (12) by least-squares fitting using the Levenberg–Marquardt algorithm.[61,62]

Figure 6 shows the $I_{corr}(q)$ versus q curves of the PA6,12/EVA blends mixed at 200 °C with and without DCP, corrected for background by the Vonk method. The determination coefficients of the experimental data fittings were ~0.99. Experimentally, I_{corr} scaled as $q^{-4.3}$ in the sample without DCP and as $q^{-5.2}$ in samples containing 8 phr DCP. The scales of the remaining samples were intermediate between these two values. Porod's Law describes the behavior of an ideal material, in which I_{corr} scales as q^{-4}. Negative deviations from Porod's law [$I(q) \sim q^{-\alpha}$, with $\alpha > 4$] have been observed in compatible polymer blends.[59,63] Blends with positive deviations from Porod's law represent fractal surfaces ($3 < \alpha < 4$).[64] The present PA6,12/EVA blends behaved as though a compatibilizer had been added due to PA6,12/EVA as discussed above.

The interfacial thicknesses of PA6,12/EVA blend depended on the DCP content. As shown in Figure 7, the thickness increased from 1.8 nm in the sample without DCP to 2.7 nm in the sample with 8 phr DCP. A trend line (B-spline) has been added to help the experimental data visualization. Due to the immiscible nature of PA6,12/EVA, well-defined phase boundaries were obtained. The increased viscosity caused by the crosslinking reaction enhanced the phase separation.

The lamellar long period is associated with the long-range-ordered structures formed in the polymer.[65] The lamellar long period L_p can be estimated from the Bragg relationship [(eq. (7)].[44] All SAXS profiles as a function of temperature are showed in Supporting Information.

In all 50/50 blends, lamellar structures started forming at approximately 160 °C, close to the temperature of pure polyamide (see Fig. 8). At all temperatures, the long period was shorter in pure PA6,12 than in the blends, because of the EVA crystallizes below 80 °C (see the Supporting Information). In the PA6,12/EVA blends, occurred the increasing of the amorphous

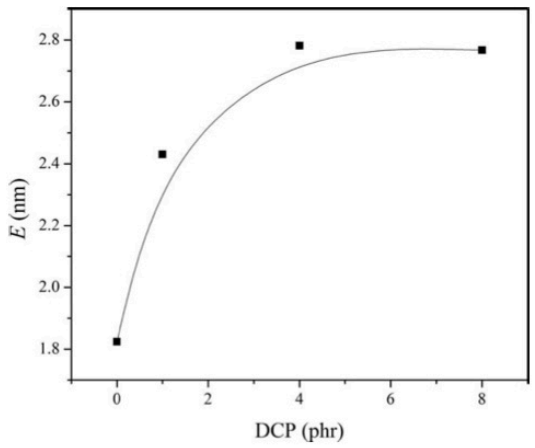

Figure 7. Interfacial thickness E in blends of PA6,12/EVA with different DCP concentrations at 200 °C.

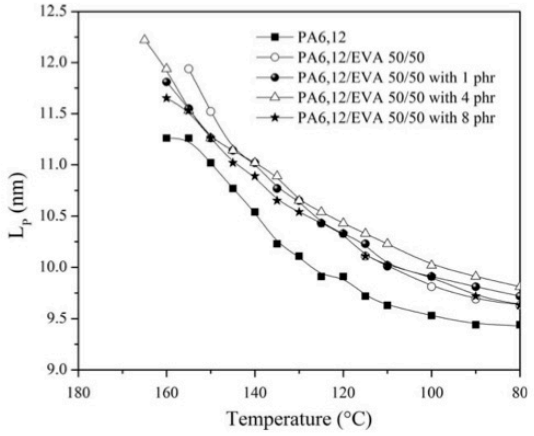

Figure 8. Lamellar long period (L_p) in PA6,12 and PA6,12/EVA blends with and without DCP.

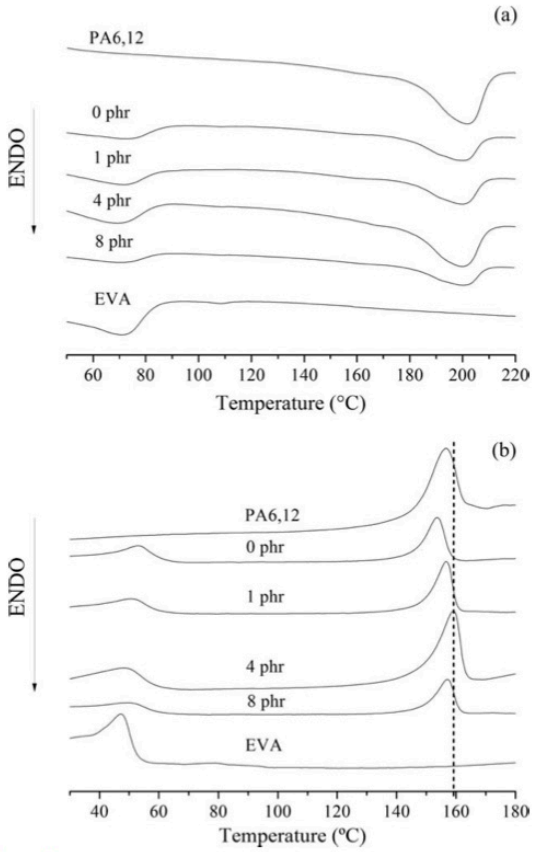

Figure 9. DSC thermograms during (a) fusion (second heating cycle) and (b) crystallization.

thickness. This trend is due to EVA becomes solid below 80 °C. This observation suggests that PA6,12 and EVA lamellae are randomly mixed above 80 °C. Similar observations are reported in literature for other polymer blends systems.[14,66,67] Thus, the size of the lamellar structure is altered by changing the constituent concentrations and type of processing, without changing the melting temperatures of the pure polymers. The same inference was made in the HDPE/EVA blends.[34]

Similar results were observed in the PA6/EVA blends compatibilized with maleic anhydride (MA). The lamellar long period increased from 8.0 nm in pure PA6 to 9.47 nm in PA6 blended with 30 wt % EVA.[14] The EVA addition increased the amorphous lamellar thickness and consequently reduced the crystalline lamellar thickness. An increased amorphous region was also observed in TPVs formed from phase decomposition polymer blends.[31]

Figure 9(a,b) presents the DSC thermograms acquired during melting and crystallization runs of the PA6,12/EVA samples, respectively. The thermogram peaks in the PA6,12/EVA blends are related to the fusion of pure polymers, which occurs regardless of DCP content. The melt temperatures of pure PA6,12 and EVA were approximately 200 and 72 °C, respectively. Table IV summarizes the melting temperatures (T_m), melting enthalpies (ΔH_m), crystallinity indexes (X_c), crystallization temperatures (T_c), and enthalpies of crystallization (ΔH_c) related to the polyamide phase of the PA6,12/EVA blends.

The broad fusion peak in the thermogram of PA6,12 [Fig. 9(a)] is the overlap of several crystalline forms with very close fusion temperatures. Specifically, both triclinic structures (α phase) and hexagonal structures (γ phase) emerge from the melt solidification of PA6,12.[68] The crystallization curves of the PA6,12/EVA blends are shown in Figure 9(b). The low-temperature (~47 °C) peak of pure EVA is attributed to the acetate in the EVA copolymer, which reduces its crystallinity.[45]

The crystallinities of the PA6,12/EVA blends were unaffected by EVA and DCP addition, resulting in similar crystallinity indexes (~22–23%). Crystallization from molten polymer/polymer or polymer/elastomer blends is complex and depends on the nature and compatibility of the melt components. The crystallization behavior of the mixture is affected by the composition, processing conditions, crystallization conditions, viscosity, surface tension, nature of dispersion, phase separation tendency, and other factors.[69] Balamurugan and Maiti[35] studied the crystallization kinetics of polyamide 6 (PA6) and the ethylene butyl acrylate (EBA) copolymer. The inclusion of the elastomeric EBA particles might obstruct the movement of the PA6 chains and change the length of the obtained crystals. When the polymer chains strongly interact, the crystallized fraction and crystallization temperature might reduce because the driving force is insufficient to exclude the amorphous fraction and form an organized phase.[70]

In this work, the EVA addition also slightly extended the crystal growth of PA6,12. However, in the present case, the interactions were too weak to change the melting, crystallization temperatures and crystallinity indexes of the PA6,12.

Dynamic Mechanical Thermal Analysis (DMTA)

Figure 10(a) plots the storage moduli *E'* of the pure components and blends as a function of temperature. The storage modulus of EVA is smaller than that of PA6,12 because the vinyl acetate groups (VA) increase the extent of the amorphous regions in the EVA copolymer.[71] The storage modulus of EVA is at least 10^3 MPa at −25 °C, and the polymer morphology is characterized by a vitreous region with a solid pseudo-elastic behavior. Above this temperature, the modulus falls to approximately 30 MPa. This large reduction reflects the significantly

Table IV. Thermal Properties of PA6,12 and Blends with and without DCP

Sample	ΔH_m	T_m (°C)	X_c (%)	T_c (°C)	ΔH_c
PA6,12	43.3	201.3	22	156.5	35.2
50/50	24.8	200.2	25	154.2	22.4
50/50 1 phr	22.2	199.8	23	156.8	19.5
50/50 4 phr	22.3	201.2	23	158.4	24.1
50/50 8 phr	22.8	199.9	23	157.6	19.4

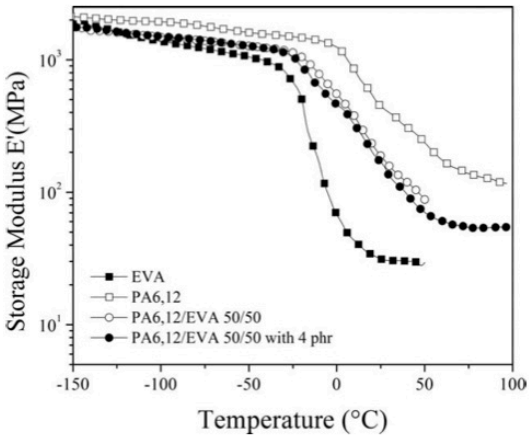

Figure 10. Storage moduli *E'* of PA6,12, EVA and their blends at 1 Hz.

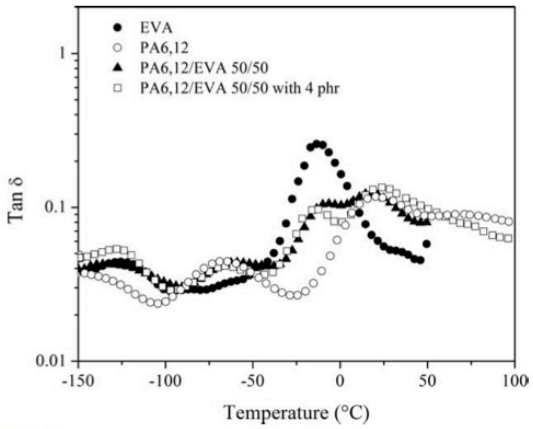

Figure 11. Tan δ of PA6,12, EVA, and 50/50 blends with 4 phr DCP and without DCP at 1 Hz.

increased in free volume in the structure caused by translational movements and rotations of the chains. Above 25 °C, an elastic plateau occurs in which the material behaves like a crosslinked elastomer. PA6,12 exhibits the same viscoelastic regions, but the elastic plateau occurs at higher temperatures than in the EVA copolymer.

The three peaks in Figure 11 are related to the primary and secondary transitions in polyamide.[65,72] In PA6,12, the α, β, and γ transitions occurs at relaxation temperatures of 20, −67, and −146 °C, respectively. The α relaxation peak indicates breakage of the hydrogen bonds between the polymer chains (CO–NH groups), which shifts the chain segments in the amorphous region of the polymer. This transition is assigned to the glass transition temperature of PA6,12. The β relaxation indicates the movement of segments involving nonhydrogen-bonded amide groups. The γ relaxation shows the onset of cooperative motions of the CH_2 groups between the amide linkages in the amorphous fractions. This relaxation occurs in all polymers.[6,65,73]

The γ relaxation peak for EVA appears at −126 °C.[74] The VA groups and elastomeric behavior introduced a small crystallinity which contributes to the β (glass) transition of EVA. Therefore, the glass transition of EVA occurs at a lower temperature and with greater intensity than those of other polyethylene compounds. Polymers such as polyethylene undergo a transition α_c associated with the crystalline lamella, not with the glass transition of the polymer.[20]

The relaxation behavior of the 50/50 blends is intermediate between those of the two pure polymers, regardless of peroxide content. Bondan and Soares[6] studied the dynamic crosslinking in PA12/EVA, varying the polymer ratios and crosslinking agent amounts. They observed glass transitions of the pure components, regardless of the composition and DCP content. This behavior typifies immiscible polymer blends.[75] However, although the pure constituents undergo glass transitions, the blended pair PA6,12/EVA exhibits a certain compatibility through the interactions between amide and acetate groups, as previously shown in the FTIR data. Table V shows the glass transition temperatures determined at 1 Hz and the average storage moduli at 23 °C determined at multiple frequencies (1, 5, 10, 20, and 50 Hz). In all blends, the glass transitions of the PA6,12 and EVA phases occurred between 16.1 and 24.4 °C and between −13 and −7.5 °C, respectively. This difference is related to the morphology of the system, as the viscoelastic response of such a system depends on the phase size and crosslinking density.[76]

As the DCP content increased in the PA6,12/EVA blends, the average storage moduli at 23 °C tended to decrease. The reductions were nonadditive due to the coarse phase morphology developed in the system. The averages of the tan δ obtained at multiple frequencies and 23 °C were similar in all blends.

The activation energy, which is related to molecular mobility, was calculated for the various PA6,12/EVA blends by eq. ((13):

$$\ln f = \ln C - \frac{E_a}{RT}, \tag{13}$$

where f is the frequency, C is a constant, and E_a is the mobility activation energy. Here, R is the universal gas constant, and T is the temperature (in K) of the peak in the tan δ curve.

Table VI presents the activation energies related to molecular mobility. All correlation coefficients exceeded 0.995. In the PA6,12/EVA blends without peroxide, the activation energy of

Table V. Glass Transitions, Storage Moduli *E'*, and Average Tan *δ* of PA6,12/AVA Blends at 23 °C

PA6-12/ EVA	DCP (phr)	$T_{g\alpha PA6\text{-}12}$ (°C)	$T_{g\beta EVA}$ (°C)	$E'_{23\ °C}$ (MPa)	$Tan\delta_{23\ °C}$
100/0	0	20	—	518.1	0.13
0/100	0	—	−13.5	32.7	0.09
50/50	0	16.7	−7.5	229.9	0.13
50/50	1	17.5	−11.1	212.1	0.13
50/50	4	24.4	−13.0	191.9	0.14
50/50	8	16.1	−13.0	200.3	0.13

the PA6,12 phase was elevated, while that of the EVA phase was reduced. This result may reflect the co-continuous morphology developed by the system.

The DCP addition reduces the viscous component mainly in the β transition region, as the formation of new C–C bonds increases the pseudo-elastic behavior of EVA.[6] Thus, effective crosslinking requires more energy for molecular mobility than when DCP is absent. These data can be correlated with the gel content analysis, in which the sample with 4 phr DCP exhibited a high gelled fraction. The blend with 8 phr peroxide demonstrated a small activation energy, which is attributed to the low crystallinity or possibly to the degradation of the system by the excessive DCP content.

Dicumyl peroxide induces a new morphology of partially fragmented EVA in the PA6,12/EVA blends. Comparing the activation energies between the crosslinked and uncrosslinked blends, we find that the activation energy was increased by adding 4 phr DCP. This result reflects the increased transition zone between the polymers, as shown in the SAXS results.

Regarding the creep behavior, the PA6,12/EVA blend without peroxide showed higher elastic recovery than the other blends because the crosslinked EVA chains impeded the mobility in the other blends. As shown in Table VII, the DCP reduced the elastic recovery. The exception was 4 phr DCP, which improved the elastic recovery to 3.4% by increasing the crosslinking phase. The recovery was reduced in samples containing 1 and 8 phr DCP, consistent with the gel content results.

Pure EVA showed higher deformation and recovery than PA6,12. The low creep recovery of pure PA6,12 reflects the low amorphous component in the semicrystalline polymers.[26] However, the high deformation and recovery of EVA can be attributed to the temperature of the creep experiment (50 °C, close to the melting temperature of EVA, as shown in the DSC results).

Peroxide addition reduced the permanent deformation and elastic recovery of the PA6,12/EVA blends because peroxide forms a crosslinked phase and reduces the mobility of the EVA chains at 70 °C (the melting temperature). The permanent deformation of the blend containing 4 phr DCP was only 0.01%, reflecting the severe restriction of the molecular motion by the high degree of crosslinking.

The TPV phase morphology yielded large particles, as observed in the SEM images. Thus, the reduced elastic recovery is associated with the increased thermoplastic area around the elastomeric phase, which increases the required buckling force.[78]

Table VI. Mobility Activation Energies of PA6,12, EVA, and their Blends

Sample	$E_{\alpha PA612}$ (kJ mol^{-1})	$E_{\alpha\ EVA}$ (kJ mol^{-1})
PA612	321.1	—
EVA	—	428.5
50/50	346.6	319.9
1 phr	294.5	315.5
4 phr	366.6	570.5
8 phr	349.8	251.5

Table VII. Elastic Recovery and Permanent Deformation of Pure Components in PA6,12 Blends with and without DCP

Sample	Permanent deformation (%)	Elastic recovery (%)
PA6,12	1.29	0.48
50/50	32.23	9.20
50/50 1 phr	6.02	2.50
50/50 4 phr	0.01	3.40
50/50 8 phr	3.21	1.75
EVA	10.32	6.20

In a previously article,[5] we showed that the tensile stress–strain behavior of the PA 6,12/EVA blends were strongly affected by the phase morphology. The addition of DCP resulted in an increase of tensile strength for 50/50 blends. Nevertheless, blends with 8 phr of DCP had a reduction in tensile strength and elongation at break. This trend was due to the generation of the abrupt phase boundaries between PA6,12 and EVA.

CONCLUSIONS

This work investigated dynamic crosslinking in PA6,12/EVA blends in the presence of a crosslinking agent (dicumyl peroxide; DCP). The mixing was done in a bath mixer (a torque rheometer). According to the gel contents, the DCP addition established new covalent bonds (C–C) among the chains of pure EVA. In 50/50 PA6,12/EVA blends, the DCP partially fragmented the morphology in a content-dependent manner.

Increasing the DCP content improved the interfacial thickness from 1.8 to 2.7 nm because of the immiscible nature of the system. The long period of lamellar samples of pure polyamide was slightly increased in the presence of DCP.

DCP addition did not affect the crystallinity of the samples but increased the amorphous thickness of the PA6,12. The glass transition temperatures of the pure constituents, derived from the solid viscoelastic properties, were characteristic of immiscible polymer blends. The improved pseudo-elastic behavior of EVA after DCP addition was associated with greater crosslinking in the system. The activation energy in blends containing 1 and 4 phr DCP was increased by the interface formed from radical reactions. The maximum elastic recovery (3.4%) after addition of 4 phr DCP was also attributed to the increased crosslinking phase.

ACKNOWLEDGMENTS

The authors thank Mantova Industria de tubos flexíveis, Retilox química for the donation of the materials, and CAPES for a scholarship to Fabrício Bondan. This work was supported by CNPq—National Council for Scientific and Technological Development, Brazil (Grant 473402/2013-0 and 308241/2015-0). The authors also thank the Brazilian Synchrotron Light Laboratory (LNLS) for the use of scientific installations (SAXS1 beamline). J.I.A. is a member of the CICPBA, La Plata, Argentina.

REFERENCES

1. De, S. K.; White, J. R. Rubber Technologist's Handbook; Rapra Technology Limited: Shawbury, UK, **2001**.
2. Coran, A. Y.; Patel, R. *Rubber Chem. Technol.* **1980**, *53*, 141.
3. Oderkerk, J.; de Schaetzen, G.; Goderis, B.; Hellemans, L.; Groeninckx, G. *Macromolecules* **2002**, *35*, 6623.
4. Antunes, C. F.; Machado, A. V.; van Duin, M. *Eur. Polym. J.* **2011**, *47*, 1447.
5. Bondan, F.; Bianchi, O. *Sci. Cum Ind.* **2015**, *3*, 23.
6. Bondan, F. B. O.; Soares, M. R. F. *Polym. Bull.* **2014**, *71*, 15.
7. Mani, S.; Cassagnau, P.; Bousmina, M.; Chaumont, P. *Macromol. Mater. Eng.* **2011**, *296*, 909.
8. Bianchi, O.; Zattera, A. J.; Canto, L. B. *J. Elastomers Plast.* **2010**, *42*, 561.
9. Martin, G.; Barres, C.; Sonntag, P.; Garois, N.; Cassagnau, P. *Eur. Polym. J.* **2009**, *45*, 3257.
10. Chatterjee, T. W. S.; Naskar, K.; Heinrich, G. *J. Exp. Polym. Lett.* **2014**, *8*, 220.
11. Veenstra, H.; van Lent, B. J. J.; van Dam, J.; Posthuma de Boer, A. *Polymer* **1999**, *40*, 6661.
12. Bhadane, P. A.; Champagne, M. F.; Huneault, M. A.; Tofan, F.; Favis, B. D. *Polymer* **2006**, *47*, 2760.
13. Mekhilef, N.; Verhoogt, H. *Polymer* **1996**, *37*, 4069.
14. Bhattacharyya, A. R.; Ghosh, A. K.; Misra, A. *Polymer* **2001**, *42*, 9143.
15. Bianchi, O.; Martins, J. D. N.; Fiorio, R.; Oliveira, R. V. B.; Canto, L. B. *Polym. Test.* **2011**, *30*, 616.
16. Bianchi, O.; Oliveira, R. V. B.; Fiorio, R.; Martins, J. D. N.; Zattera, A. J.; Canto, L. B. *Polym. Test.* **2008**, *27*, 722.
17. Nesterov, A. E.; Lebedev, E. V. *Russ. Chem. Rev.* **1989**, *58*, 795.
18. Oliveira, R. V. B.; Ferreira, C. I.; Peixoto, L. J. F.; Bianchi, O.; Silva, P. A.; Demori, R.; Silva, R. P.; Veronese, V. B. *Polímeros* **2013**, *23*, 91.
19. Moad, G. *Prog. Polym. Sci.* **1999**, *24*, 81.
20. Faker, M.; Razavi Aghjeh, M. K.; Ghaffari, M.; Seyyedi, S. A. *Eur. Polym. J.* **2008**, *44*, 1834.
21. Robertson, R. E.; Paul, D. R. *J. Appl. Polym. Sci.* **1973**, *17*, 2579.
22. Moly, K. A.; Radusch, H. J.; Androsh, R.; Bhagawan, S. S.; Thomas, S. *Eur. Polym. J.* **2005**, *41*, 1410.
23. Reyes-Labarta, J. A.; Olaya, M. M.; Marcilla, A. *Polymer* **2006**, *47*, 8194.
24. John, B.; Varughese, K. T.; Oommen, Z.; Pötschke, P.; Thomas, S. *J. Appl. Polym. Sci.* **2003**, *87*, 2083.
25. Joubert, C.; Cassagnau, P.; Michel, A.; Choplin, L. *Polym. Eng. Sci.* **2002**, *42*, 2222.
26. Gomes, A. C. O.; Soares, B. G.; Oliveira, M. G.; Paranhos, C. M. *Polímeros* **2009**, *19*, 196.
27. Ismail, H.; Nasir, S. M. *Polym. Test.* **2001**, *20*, 819.
28. Elias, L.; Fenouillot, F.; Majeste, J. C.; Cassagnau, P. *Polymer* **2007**, *48*, 6029.
29. Wang, Y.; Zhang, Q.; Fu, Q. *Macromol. Rapid Commun.* **2003**, *24*, 231.
30. Li, Y.; Shimizu, H. *Polymer* **2004**, *45*, 7381.
31. Li, Y.; Oono, Y.; Kadowaki, Y.; Inoue, T.; Nakayama, K.; Shimizu, H. *Macromolecules* **2006**, *39*, 4195.
32. Freire, E.; Bianchi, O.; Forte, M. M. C.; Preto, M.; Monteiro, E. E. C.; Tavares, M. I. B. *Polym. Eng. Sci.* **2008**, *48*, 1901.
33. Thompson, A.; Bianchi, O.; Amorim, C. L. G.; Lemos, C.; Teixeira, S. R.; Samios, D.; Giacomelli, C.; Crespo, J. S.; Machado, G. *Polymer* **2011**, *52*, 1037.
34. Na, B.; Wang, Y.; Du, R.; Fu, Q.; Men, Y. *J. Polym. Sci. Part B: Polym. Phys.* **2004**, *42*, 1831.
35. Balamurugan, G. P.; Maiti, S. N. *J. Appl. Polym. Sci.* **2008**, *107*, 2414.
36. Van Krevelen, D. W.; Nijenhuis, K. T. Properties of Polymers; Elsevier: Oxford, **2009**.
37. Pacheco, M. F. M.; Bianchi, O. v.; Fiorio, R.; Zattera, A. J.; Zeni, M.; Giovanela, M.; Crespo, J. S. *J. Elastomers Plast.* **2009**, *41*, 323.
38. Kumar, C. R.; Nair, S. V.; George, K. E.; Oommen, Z.; Thomas, S. *Polym. Eng. Sci.* **2003**, *43*, 1555.
39. Dove, S. B. Dental Diagnostic Science; UT Health Science Center, School of Dentistry: San Antonio, TX, USA, **2002**. Available at: http://compdent.uthscsa.edu/dig/itdesc.html
40. Ruland, W. *J. Appl. Crystallogr.* **1971**, *4*, 70.
41. Vonk, C. *J. Appl. Crystallogr.* **1978**, *11*, 541.
42. Yanagioka, M.; Toney, M. F.; Frank, C. W. *Macromolecules* **2009**, *42*, 1331.
43. Bianchi, O.; Barbosa, L. G.; Machado, G.; Canto, L. B.; Mauler, R. S.; Oliveira, R. V. B. *J. Appl. Polym. Sci.* **2013**, *128*, 811.
44. Glatter, O.; Kratky, O. Small Angle X-ray Scattering; Academic Press: London, UK, **1982**.
45. Shi, X. M. Z. J. J.; Chen, J. J. S. *eXPRESS Polym. Lett.* **2008**, *2*, 623.
46. Elzein, T.; Brogly, M.; Schultz, J. *Polymer* **2002**, *43*, 4811.
47. Bousmina, M.; Ait-Kadi, A.; Faisant, J. B. *J. Rheol.* **1999**, *43*, 415.
48. Bianchi, O.; Fiorio, R.; Martins, J. N.; Zattera, A. J.; Scuracchio, C. H.; Canto, L. B. *J. Elastomers Plast.* **2009**, *41*, 175.
49. Jha, A.; Bhowmick, A. K. *J. Appl. Polym. Sci.* **1998**, *69*, 2331.
50. Khonakdar, H. A.; Jafari, S. H.; Yavari, A.; Asadinezhad, A.; Wagenknecht, U. *Polym. Bull.* **2005**, *54*, 75.
51. Owens, D. K.; Wendt, R. C. *J. Appl. Polym. Sci.* **1969**, *13*, 1741.
52. Guggenheim, E. A. *J. Chem. Phys.* **1945**, *13*, 253.
53. Huang, H.; Liu, X.; Ikehara, T.; Nishi, T. *J. Appl. Polym. Sci.* **2003**, *90*, 824.
54. Földes, E.; Pukánszky, B. *J. Colloid Interface Sci.* **2005**, *283*, 79.
55. Belke, R. E.; Cabasso, I. *Polymer* **1988**, *29*, 1831.
56. Tsebrenko, I. A.; Pakharenko, V. A. *Fiber Chem.* **1999**, *31*, 197.

57. Svergun, D. I. L. A. F. Structure Analysis by Small-Angle X-ray and Neutron Scattering; Plenun Press: New York, **1987**.
58. Vonk, C. *J. Appl. Crystallogr.* **1971**, *4*, 340.
59. Perrin, P.; Prud'homme, R. E. *Macromolecules* **1994**, *27*, 1852.
60. Becker, D.; Porcel, F.; Hage, E., Jr.; Pessan, L. *Polym. Bull.* **2008**, *61*, 353.
61. Marquardt, D. W. *J. Soc. Ind. Appl. Math.* **1963**, *11*, 431.
62. Levenberg, K. *Quart. Appl. Math.* **1944**, *2*, 164.
63. Li, L.; Lambreva, D.; de Jeu, W. H. *J. Macromol. Sci. B* **2005**, *43*, 59.
64. Brinker, K. L.; Lebovitz, A. H.; Torkelson, J. M.; Burghardt, W. R. *J. Polym. Sci. Part B: Polym. Phys.* **2005**, *43*, 3413.
65. Ernzen, J. R.; Bondan, F.; Luvison, C.; Henrique Wanke, C.; De Nardi Martins, J.; Fiorio, R.; Bianchi, O. *J. Appl. Polym. Sci.* **2016**, *133*, 43050.
66. Chen, H. L.; Hsiao, M. S. *Macromolecules* **1998**, *31*, 6579.
67. Bose, S.; Bhattacharyya, A. R.; Kodgire, P. V.; Misra, A.; Pötschke, P. *J. Appl. Polym. Sci.* **2007**, *106*, 3394.
68. Ramesh, C. *Macromolecules* **1999**, *32*, 3721.
69. Martuscelli, E. *Polym. Eng. Sci.* **1984**, *24*, 563.
70. Freire, E.; Bianchi, O.; Martins, J. N.; Monteiro, E. E. C.; Forte, M. M. C. *J. Non-Cryst. Solids* **2012**, *358*, 2674.
71. Sung, Y. T.; Kum, C. K.; Lee, H. S.; Kim, J. S.; Yoon, H. G.; Kim, W. N. *Polymer* **2005**, *46*, 11844.
72. Serpe, G.; Chaupart, N. *J. Polym. Sci. Part B: Polym. Phys.* **1996**, *34*, 2351.
73. Kohan, M. I. Nylon Plastics Handbook; Hanser: New York, **1995**.
74. Schatzki, T. F. *J. Polym. Sci.* **1962**, *57*, 337.
75. Bhattacharyya, A. R.; Maiti, S. N.; Misra, A. *J. Appl. Polym. Sci.* **2002**, *85*, 1593.
76. Komalan, C.; G. K. E.; Kumar, P. A. S; Varughese, K. T.; Thomas, S. *eXPRESS Polym. Lett.* **2007**, *1*, 641.
77. Gedde, U. W. Polymer Physics; Kluwer Academic Publisher: Dordercht, **1995**.
78. Wu, S. *Polymer* **1985**, *26*, 1855.